Parametric Study of Airframe-Integrated Scramjet Cooling Requirement

Takeshi Kanda,* Goro Masuya,† Yoshio Wakamatsu,† Nobuo Chinzei,‡ and Akio Kanmuri§
National Aerospace Laboratory, Kakuda, Miyagi, Japan

In a previous report, scramjet engine characteristics of different propellant-fed cycles were compared and engine performances were discussed. In this study, the cooling requirement of a hydrogen-fueled airframe-integrated scramjet engine as well as an airframe was examined, and effects of various parameters including flight Mach number, flight dynamic pressure, engine wall temperature, and engine scale, on the engine characteristics were analyzed. The coolant required for the airframe was about 20% of the total coolant. Simple equations that correlate coolant flow rate with those parameters were derived.

Nomenclature

A = cross-sectional area
B = constant in Eq. (5)
b = exponent in Eq. (5)
C_D = drag coefficient
C_p = specific heat at constant pressure
h = heat transfer coefficient
I_{sp} = specific impulse
ℓ = representative length
M = Mach number
$\dot{m}$ = mass flow rate
P = pressure
$\dot{Q}$ = heat transfer rate
q = dynamic pressure
S_t = Stanton number
T = temperature
u = stream velocity
V = flight velocity
W = power
γ = specific heat ratio
ΔT = difference between wall temperature and total temperature
ΔT_{cl} = increase of coolant temperature
ΔT_r = increase of temperature by chemical reaction
η = efficiency
λ = friction coefficient
μ = viscosity
ρ = density

Subscripts

AF = airframe
cl = coolant
cp = captured
E = engine
f = fuel
fp = fuel pump
g = combustion gas
H2 = hydrogen
p = pump
st = stoichiometric
t = turbine
w = wall
0 = total
1 = entrance, entrance of inlet
2 = exit
∞ = freestream

Received May 17, 1989; revision received Dec. 4, 1989. Copyright © 1990 by the American Institute of Aeronautics and Astronautics, Inc. All rights reserved.

*Researcher, Kakuda Research Center.
†Senior Researcher, Kakuda Research Center.
‡Head, Ramjet Performance Section, Kakuda Research Center.
§Head, Rocket Engine Systems Section, Kakuda Research Center.

I. Introduction

In our previous reports[1,2] of an airframe-integrated scramjet engine, power cycle consideration, regenerative cooling requirement, and performances with a flight path along a constant dynamic pressure of 100 kPa were discussed.

An aerospace plane is assumed to fly along a path of constant flight dynamic pressure. Therefore, the selection of flight dynamic pressure is important. On the other hand, active cooling should be considered in order to protect the airframe from severe aerodynamic heating due to high flight Mach number. In the process of scramjet development, the effect of scale is also important. However, there are few reports that mention these effects, i.e., flight dynamic pressure[3] and airframe cooling.[4]

In this study, parametric calculation of the cooling requirement for a hydrogen-fueled airframe-integrated scramjet engine as well as an airframe was carried out.

Simplified explicit correlations between the coolant flow rate and the various factors, i.e., flight Mach number, flight dynamic pressure, engine wall temperature, and engine scale were derived. The correlations were then compared with the results of the numerical calculation.

II. Numerical Calculation

A. Calculation Methods

Calculation methods were almost the same as those used in the previous reports.[1,2] For the given configuration of the airframe and the engine, flow properties around the airframe and inside the air-breathing part of the engine were calculated by the quasi-one-dimensional approach with assumed temperature and flow rate of fuel. The heat transfer coefficient along the wall with constant surface temperature was calculated to evaluate heat transfer to the cooling jackets. The temperature and flow rate of fuel were iteratively determined so that those assumed for flow property calculation agreed with those determined from the cooling requirement. Finally, the pressure level of pumps, turbines, and feedlines was determined by consideration of the power balance of a turbopump system. An outline of each process is described below.

1. *Configuration of Airframe and Engine System*

Configuration of the airframe was assumed as shown in Fig. 1. An airframe-integrated scramjet engine was composed of six engine modules mounted on the airframe. The module consists of an air-breathing part and a propellant feed part. The configuration of the module is shown in Fig. 2, which is based on the NASA Langley model[3] as can be seen.

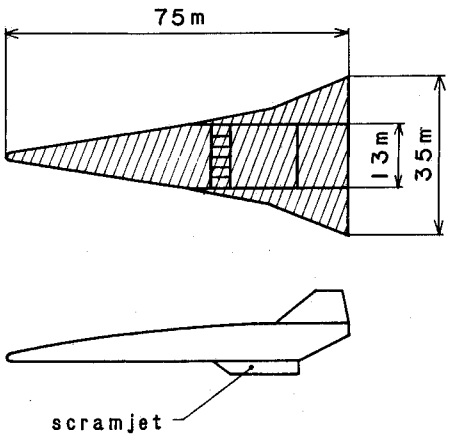

Fig. 1 Airframe configuration.

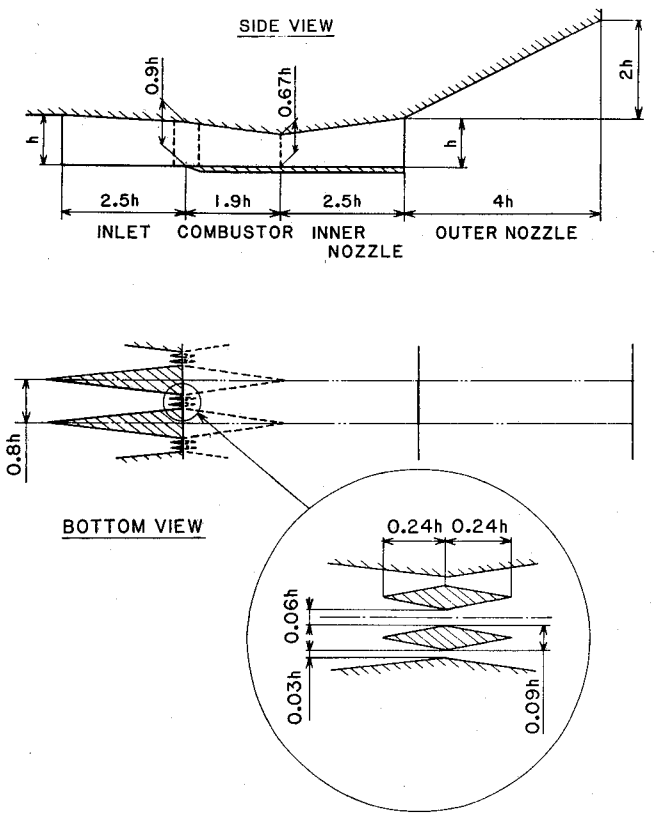

Fig. 2 Engine configuration (air-breathing part).

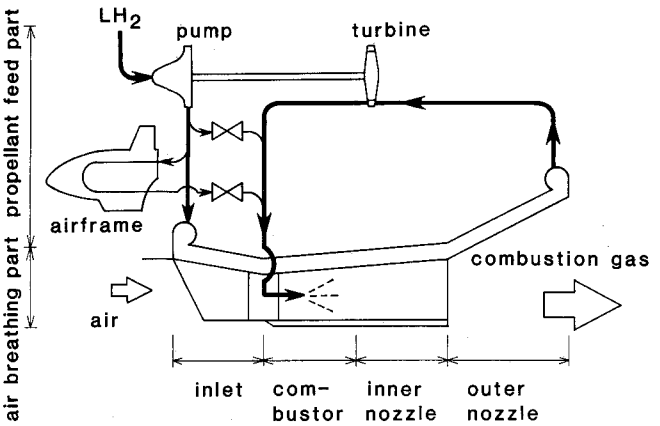

a) Expander cycle

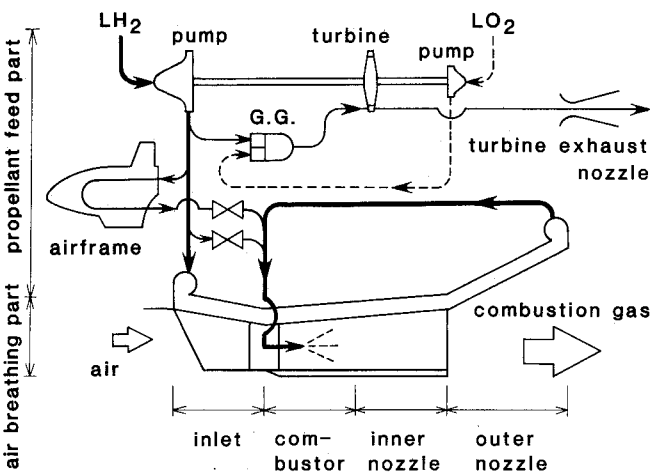

b) Gas generator cycle

Fig. 3 Engine cycle schematic.

An expander cycle (EC) and a gas generator cycle (GGC) were employed for the propellant feed part in this analysis. Both are typical in rocket engines, and their turbopump technology is available. It has been shown that the EC is simple and has a high specific impulse, whereas the GGC has been widely used in rocket engines and is characterized by flexibility of operation. The schematics of the EC and the GGC are shown in Figs. 3a and 3b, respectively. Hydrogen was used as fuel and coolant. Turbine driving gas of the GGC was exhausted through a nozzle that has an exit/throat area ratio of 10. Onboard oxygen was used as oxidizer for the gas generator.

The air-breathing part of each module and the undersurface of the fuselage and of the wings, shown by hatched lines in Fig. 1, were actively cooled with hydrogen. The cooling jacket is assumed to use tubes.

All of the coolant was injected into the combustors. For the low cooling requirement, additional fuel was injected to maintain the equivalence ratio in the air-breathing part at unity. When the coolant flow rate surpassed the stoichiometric flow rate, the equivalence ratio became greater than unity.

2. Flow in the Air-Breathing Part

Flow around the airframe and in the air-breathing part of the engine was computed by a quasi-one-dimensional scramjet performance prediction program.[5] The forebody was approximated by a cone with a half-angle of 5 deg, and the inviscid flow around it was calculated.

Empirical relations derived from experimental results[6,7] were used to evaluate the capture area ratio of the inlet. Total pressure recovery efficiency of the inlet was calculated by assuming a constant kinetic energy efficiency of 0.98 based on the experimental data.[6,7]

For the combuster and the inner nozzle, a set of quasi-one-dimensional equations[8] including effects of cross-sectional area change, chemical reaction, skin friction, and heat transfer were numerically integrated with assumed combustion efficiency distribution. An empirical relation of mixing efficiency proposed by Northam and Anderson[9] was used as the combustion efficiency.

Exhaust from the inner nozzle was assumed to expand on the afterbody or the outer nozzle to the same pressure as that on the forebody surface.

3. Heat Transfer and Cooling

In the calculation of heat transfer, it was assumed that the turbulent boundary layers started at the entrance of the inlet in the air-breathing part, at the nose of the fuselage, and at the leading edges of the wings.

Actually, laminar boundary layers may develop in the initial wall regions. However, the transition criteria for the hypersonic boundary layer is not well understood. Thus the

boundary layers were assumed to be turbulent throughout. This assumption would cause overestimation of the cooling requirement because of lower heat transfer of laminar boundary layers.

High local heat transfer is observed at the leading edge or the nose. This is an important problem for local cooling. However, this effect has negligible influence on the total cooling requirement because the area of high local heat transfer is very small compared with the whole cooled surface area.

The wall temperature along the air-breathing part and the airframe was set constant and uniform for an assumed wall material. More realistic nonuniform wall temperature distribution would result in slightly higher heat transfer.[3]

The hydrogen temperature at the exit of the cooling jacket was set at 700 K in the engine and at 300 K in the airframe. The latter value was set in consideration of payload or inside environment, especially for the case of manned missions.

Mayer's method[10] was used to calculate the heat transfer coefficient. Thermochemical and transport properties of hydrogen and oxygen in gas and liquid phases and their combustion products were calculated with a high-speed computation code[11] developed for LH_2/LO_2 rocket engine analysis.

4. Power Balance in Propellant Feed Part

The pressure level of the propellant feed part of the engine was determined so that the fuel could be injected into the combustor with suitable dynamic pressure to achieve good penetration into the airstream. The dynamic pressure ratio of fuel jet to airstream at the fuel injection position was set at unity.[12] The fuel was assumed to be injected at the sonic speed. Required values of pressure at the turbine exit P_{t2} for the EC and at the pump exit P_{p2} for the GGC were then calculated by adding various pressure drops to the fuel injection pressure.

The pressure drop in the tubes of the cooling jacket was calculated, taking friction and acceleration by expansion during heat exchange into consideration.[13] Pressure drops in feedlines were also calculated based on examples of the rocket engines.[14]

Feed cycle power balance is achieved when the power produced by the turbine equals that required by the pump. Each power was calculated by the following equations[13]:

$$W_t = \eta_t \dot{m}_t C_p T_{t1} \left[1 - \left(\frac{P_{t2}}{P_{t1}} \right)^{\frac{\gamma-1}{\gamma}} \right] \tag{1}$$

$$W_p = \frac{\dot{m}_p (P_{p2} - P_{p1})}{\eta_p \rho_{p1}} \tag{2}$$

Equations (1) and (2) were solved by iteration to evaluate the pump exit pressure P_{p2} for the EC or the turbine flow rate $\dot{m}_t$ for the GGC. Since the EC is a closed cycle, the turbine flow rate and the pump flow rate $\dot{m}_p$ are the same. In the GGC, pressure in the turbine exit manifold had no direct relation with the fuel injection pressure and was set to maintain an underexpanded condition of the turbine exhaust nozzle. The turbine entrance gas temperature T_{t1} of the GGC was set at 850 K, while that of the EC was obtained from the heat transfer calculation.

Efficiencies of the pump and the turbine in Eqs. (1) and (2) were estimated on the basis of typical values for turbopumps of rocket engines, because the operating condition of scramjet engine turbopumps would be similar to that of rocket engine turbopumps. Efficiency of the hydrogen pump was 60%, whereas that of the oxygen pump that was used in the GGC was 40%. The turbine of the EC was assumed to be a reaction turbine with efficiency of 60%, whereas that of the GGC was assumed to be an impulse turbine with efficiency of 30%. Pump entrance pressure P_{p1} is set to 0.2 MPa for hydrogen and 0.3 MPa for oxygen to avoid cavitation in the pumps.

5. Parameters

Parametric calculation for the flight conditions was carried out in the range of flight Mach numbers from 6 to 12 and of flight dynamic pressures from 25 to 150 kPa. These are considered to be typical operating ranges of a scramjet. The reference flight dynamic pressure was chosen to be 100 kPa.

The effect of the wall temperature along the air-breathing part and the airframe in the range from 700 to 2500 K was discussed. The reference wall temperature was set at 1000 K, considering the use of nickel alloy for the wall material. The maximum temperature of 2500 K was chosen because this value might be achieved by an advanced refractory material program in progress.[15]

The reference value of the module frontal area was chosen to be 6 m^2. The length scale of the engine was varied by tenfold and, thus, the frontal area by a hundredfold.

B. Results and Discussion

1. Flight Mach Number

The hydrogen flow rate of the GGC at a flight dynamic pressure of 100 kPa is shown in Fig. 4a, which is the total of the six modules. The coolant flow rate for the airframe is about 20% of the total coolant flow rate $\dot{m}_{cl}$. The total coolant flow rate surpasses the stoichiometric flow rate $\dot{m}_{st}$ at a flight Mach number of about 10.

The EC, $\dot{m}_{cl}$ and $\dot{m}_{st}$ are the same as those for the GGC in Fig. 4a. However, the total cycle flow rate for the GGC $\dot{m}_{fp}$ is greater than the EC flow rate. The difference is the flow rate into the gas generator, which is expressed as GG in Fig. 4a.

The coolant flow rate of the airframe was reported by Becker.[4] In his study, the coolant flow rate increases with flight Mach number, the same tendency as in the present study. The principle of this calculation method is basically the same as that of the present method. He determined the ratio of the heat transferred from hot gas to an airframe Q_{AF} to the heat capacity of coolant $\dot{Q}_f$:

$$\frac{\dot{Q}_{AF}}{\dot{Q}_f} = 0.00031 \frac{S_t}{C_D} \frac{I_{sp} V}{\Delta T_{cl}} \left(1 - \frac{T_w - T_\infty}{0.00007 V^2} \right) \tag{3}$$

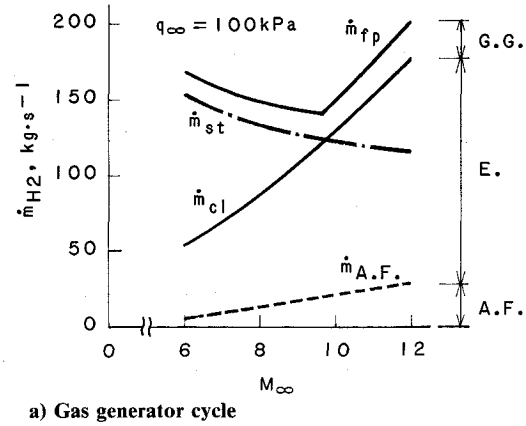

a) Gas generator cycle

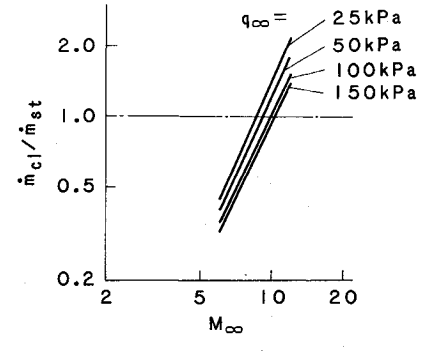

b) Coolant flow ratio ($\dot{m}_{cl}/\dot{m}_{st}$)

Fig. 4 Hydrogen flow rate with flight Mach number.

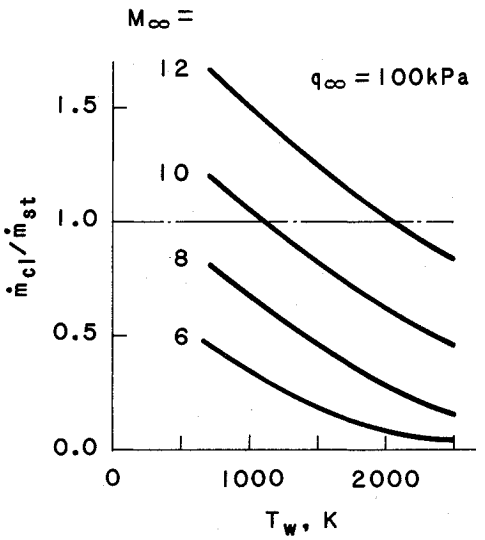

Fig. 5 Coolant flow ratio with wall temperature.

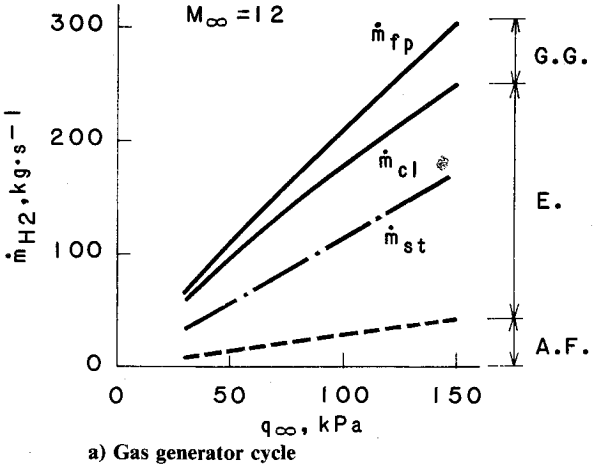

a) Gas generator cycle

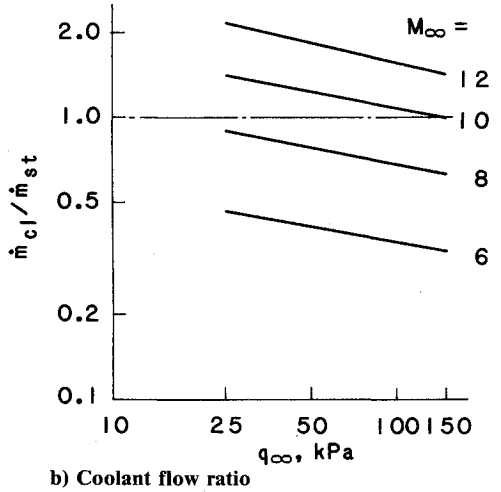

b) Coolant flow ratio

Fig. 6 Hydrogen flow rate with flight dynamic pressure.

He assumed that only the fuel was used in the engine as coolant and turbopump driving gas and did not assume the use of onboard oxidizer in the engine.

In the following discussion, the ratio of the coolant flow rate to the stoichiometric flow rate is termed as the "coolant flow ratio." The coolant flow ratio plotted with the flight Mach number is shown in Fig. 4b. The coolant flow ratio increases with the flight Mach number and with the decrease of flight dynamic pressure. This tendency is the same as in Buchmann's study.[3]

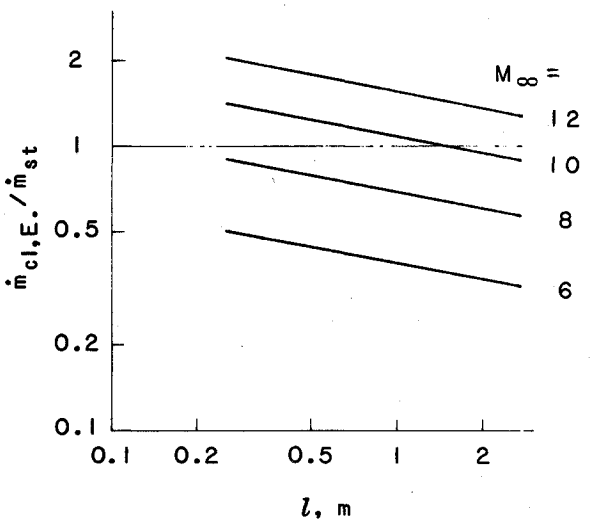

Fig. 7 Coolant flow ratio with engine scale.

2. Wall Temperature

The relation between the coolant flow ratio and the wall temperature is shown in Fig. 5, where the flight Mach number and flight dynamic pressure are constant. In the case of an engine with high wall temperature, the wall is assumed to be made of advanced refractory material with low thermal conductivity. The coolant flow ratio shows a nearly linear decrease with the increase in wall temperature.

3. Flight Dynamic Pressure

The hydrogen flow rate of the GGC plotted with flight dynamic pressure at a flight Mach number of 12 is shown in Fig. 6a. The increase of the pressure in the engine with flight dynamic pressure causes the coolant flow rate to increase with flight dynamic pressure. The increase of the incoming flow rate with flight dynamic pressure is the reason why the stoichiometric flow rate increases with flight dynamic pressure.

The ratio of the GGC to total flow rate increases with flight dynamic pressure. This tendency is also observed in other Mach number regions. This is because the power required for the pump becomes larger due to the increase in pump exit pressure with higher flight dynamic pressure. The increase of pump exit pressure with flight dynamic pressure is mainly due to the constant value of the fuel/air injection dynamic pressure ratio.

The coolant flow ratio is shown in Fig. 6b with the flight dynamic pressure. The coolant flow ratio decreases with the flight dynamic pressure.

4. Engine Scale

The scale effect for the engines with similar geometries is shown in Fig. 7. The representative length, ℓ, is the height at the entrance of the inlet. In this consideration, the cooling of the engine alone is taken into account. The coolant flow ratio decreases with the increase of engine scale.

III. Simplified Correlations

A. Derivation

If the cooling passage exit temperature of hydrogen coolant is fixed from the standpoint of allowable temperature of material, the hydrogen flow rate required for cooling is proportional to the heat flux

$$\dot{m}_{cl} \propto \dot{Q} \propto h \Delta T \ell^2 \tag{4}$$

The ℓ^2 represents the heat exchanging area, whereas ℓ is representative length. As for the gas side heat transfer coefficient h, the Reynolds analogy was used in this analytical approach, which is the basis of Mayer's method.[10] The skin-friction

coefficient on a flat plate λ is derived from Blasius' empirical formula[16] as follows:

$$\lambda/2 = B(\rho u \ell/\mu)^{-b} \tag{5}$$

In case of turbulent flow on a flat plate, b is 0.2.[10,16] The Reynolds analogy is rewritten as follows:

$$S_t \equiv h/\rho u C_p = \lambda/2 \tag{6}$$

As can be seen from the above two equations, the heat transfer coefficient is proportional to the 0.8 power of the product of density and velocity

$$h \propto (\rho u)^{0.8} = [\eta_{cp}\rho_\infty u_\infty (A_\infty/A)]^{0.8} \tag{7}$$

where A is the cross-sectional area at the air-breathing part, and A_∞ represents the cross-sectional area of the freestream, which flows into the engine. The η_{cp} is a capture area ratio, which is a function of a Mach number.[6,7] They are illustrated in Fig. 8. In the following, the projected cross-sectional area at the entrance of the inlet A_1 is chosen as the representative area of A. The A_∞/A_1, which is calculated based on Refs. 8 and 17, is proportional to the 0.5 power of the flight Mach number from 6 to 12.

The heat transfer coefficient can also be derived to be proportional to the -0.2 power of the length ℓ from Eqs. (5) and (6):

$$h \propto \ell^{-0.2} \tag{8}$$

From Eqs. (7) and (8), we can derive the following relation:

$$h \propto [\eta_{cp}\rho_\infty u_\infty (A_\infty/A_1)]^{0.8}\ell^{-0.2} \tag{9}$$

Next, ΔT is examined. Total temperature is used in the following in place of adiabatic wall temperature to simplify the discussion, because the total temperature is nearly equal to the adiabatic wall temperature. The total temperature of combustion gas T_{g0} is affected by the contribution of the chemical reaction (combustion) ΔT_r and by the contribution of the total temperature of incoming air into the air-breathing part:

$$T_{g0} \propto T_\infty \left(1 + \frac{\gamma-1}{2} M_\infty^2\right) + \Delta T_r \tag{10}$$

The difference between the wall temperature and the total temperature is as follows:

$$\Delta T = T_{g0} - T_w \propto T_\infty \left\{\frac{\gamma-1}{2} M_\infty^2 + \left(1 + \frac{\Delta T_r}{T_\infty} - \frac{T_w}{T_\infty}\right)\right\} \tag{11}$$

In this study, the 1962 U.S. Standard Atmosphere was adopted to evaluate the freestream static temperature and static pressure. Along the trajectories of the aerospace plane discussed here, which is between 20 and 40 km in altitude, the value of the freestream static temperature T_∞ varies from 216 to 250 K, and the corresponding relative change in speed of sound is less than 8%. Therefore, the flight Mach number M_∞ is nearly proportional to the flight velocity u_∞. The coolant flow rate is derived as follows:

$$\dot{m}_{cl} \propto \left[\eta_{cp}\rho_\infty u_\infty \left(\frac{A_\infty}{A_1}\right)\right]^{0.8} \ell^{-0.2} T_\infty \left[\frac{\gamma-1}{2} M_\infty^2 + \left(1 + \frac{\Delta T_r}{T_\infty} - \frac{T_w}{T_\infty}\right)\right] \ell^2 \times \propto \eta_{cp}^{0.8} q_\infty^{0.8} \ell^{1.8} \left(\frac{A_\infty}{A_1}\right)^{0.8} \left[\frac{\gamma-1}{2} M_\infty^{1.2} + \left(1 + \frac{\Delta T_r}{T_\infty} - \frac{T_w}{T_\infty}\right) M_\infty^{-0.8}\right] \tag{12}$$

The stoichiometric flow rate is proportional to the airflow rate:

$$\dot{m}_{st} \propto \eta_{cp}\rho_\infty u_\infty \left(\frac{A_\infty}{A_1}\right)\ell^2 \propto \eta_{cp} q_\infty M_\infty^{-1} \left(\frac{A_\infty}{A_1}\right)\ell^2 \tag{13}$$

The coolant flow ratio is as follows:

$$\frac{\dot{m}_{cl}}{\dot{m}_{st}} \propto \eta_{cp}^{-0.2} q_\infty^{-0.2} \left(\frac{A_\infty}{A_1}\right)^{-0.2} \ell^{-0.2} \left[\frac{\gamma-1}{2} M_\infty^{2.2} + \left(1 + \frac{\Delta T_r}{T_\infty} - \frac{T_w}{T_\infty}\right) M_\infty^{0.2}\right] \tag{14}$$

Next, each relation is examined, i.e., with flight Mach number, wall temperature, flight dynamic pressure, and engine scale.

B. Effects of Parameters

1. Flight Mach Number and Wall Temperature

When flight dynamic pressure, wall temperature, and engine scale are constant, respectively, the coolant flow rate and the stoichiometric flow rate are derived as follows from Eqs. (12) and (13), respectively:

$$\dot{m}_{cl} \propto \eta_{cp}^{0.8} M_\infty^{-0.8} \left(\frac{A_\infty}{A_1}\right)^{0.8} \left[\frac{\gamma-1}{2} M_\infty^2 + \left(1 + \frac{\Delta T_r}{T_\infty} - \frac{T_w}{T_\infty}\right)\right] \tag{15}$$

$$\dot{m}_{st} \propto \eta_{cp} M_\infty^{-1} \left(\frac{A_\infty}{A_1}\right) \tag{16}$$

The coolant flow ratio is as follows:

$$\frac{\dot{m}_{cl}}{\dot{m}_{st}} \propto \eta_{cp}^{-0.2} M_\infty^{0.2} \left(\frac{A_\infty}{A_1}\right)^{-0.2} \left[\frac{\gamma-1}{2} M_\infty^2 + \left(1 + \frac{\Delta T_r}{T_\infty} - \frac{T_w}{T_\infty}\right)\right] \tag{17}$$

The measured capture area ratios are more than 0.9 for a flight Mach number range of 6 to 10.[6,7] Although the capture area ratio is a function of a flight Mach number, $\eta_{cp}^{-0.2}$ in Eq. (17) is almost constant for the flight Mach number range considered in the present study.

The dependence of the coolant flow ratio on flight Mach number is influenced by the magnitude of the term $(\gamma-1)M_\infty^2/2$, relative to the term $(1 + \Delta T_r/T_\infty - T_w/T_\infty)$. On the other hand, the term ΔT_r is zero in Eq. (17) when there is no chemical reaction, so the effect of ΔT_r is reduced when the whole engine is examined. For example, the hydrogen cooling the noncombustion parts, i.e., the inlet and the airframe, amounts to 40% of the total hydrogen flow rate. According to the comparison of the preceding two terms, the term

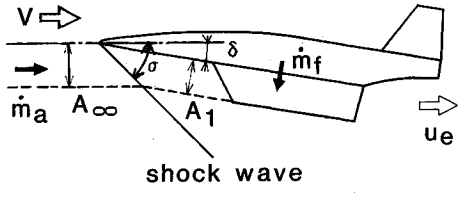

Fig. 8 Flight condition.

$(\gamma-1)\,M_\infty{}^2/2$ in Eq. (17) is much larger than the other term $(1+\Delta T_r/T_\infty - T_w/T_\infty)$, and the coolant flow ratio is proportional to the 2.2 power of the flight Mach number when the wall temperature is 1000 K. This analytical result is confirmed from Fig. 4b, which is based on the exact heat transfer calculation.

The term $(1+\Delta T_r/T_\infty - T_w/T_\infty)$, however, becomes comparable with the term $(\gamma-1)M_\infty^2/2$ when the flight Mach number is low, or, for example, a higher wall temperature is possible with use of highly refractory wall material. Thus the coolant flow ratio is no longer proportional to the 2.2 power of the flight Mach number.

The relation between the coolant flow ratio and the wall temperature is shown as the following equation:

$$\dot{m}_{cl}/\dot{m}_{\rm st} \propto C - T_w \tag{18}$$

where C is a constant. Equation (18) agrees with the calculated result as shown in Fig. 5.

2. Flight Dynamic Pressure

In the condition that the flight Mach number is constant, the properties, e.g., temperature, in the air-breathing part do not vary with flight dynamic pressure in the region under discussion here. Therefore, the coolant flow rate and the stoichiometric flow rate are derived as follows from Eqs. (12) and (13) when flight Mach number, wall temperature, and engine scale are constant:

$$\dot{m}_{cl} \propto q_\infty^{0.8} \tag{19}$$

$$\dot{m}_{\rm st} \propto q_\infty \tag{20}$$

The coolant flow ratio is derived as follows, and it agrees with the calculation result shown in Fig. 6b:

$$\dot{m}_{cl}/\dot{m}_{\rm st} \propto q_\infty^{-0.2} \tag{21}$$

3. Engine Scale

When flight Mach number, flight dynamic pressure, and wall temperature are constant, the coolant flow rate and the stoichiometric flow rate with the engine scale are as shown below from Eqs. (12) and (13):

$$\dot{m}_{cl} \propto \ell^{1.8} \tag{22}$$

$$\dot{m}_{\rm st} \propto \ell^2 \tag{23}$$

The coolant flow ratio is as follows:

$$\dot{m}_{cl}/\dot{m}_{\rm st} \propto \ell^{-0.2} \tag{24}$$

The coolant flow ratio is proportional to the -0.2 power of the representative length, and it agrees with the calculated result shown in Fig. 7.

Although, in this case, the coolant for airframe cooling is excluded from the total coolant flow rate as mentioned before, the above relations are valid for the engine and airframe if the scale of the airframe and that of the engine varies proportionally.

IV. Conclusions

Parametric calculation on cooling requirement for an airframe and a scramjet engine of an aerospace plane was carried out. Analytical relationships were derived and compared with the calculated results. The following has been made clear from the investigation.

1) The hydrogen flow rate required for airframe regenerative cooling is about 20% of the total hydrogen flow rate for cooling in this study.

2) The influences on hydrogen flow rate from various parameters, e.g., flight Mach number, were made clear by the parametric calculation.

3) The correlation among the coolant flow rate, stoichiometric flow rate, flight Mach number, flight dynamic pressure, wall temperature, and engine scale were derived. Thereby, the effects of those parameters on the hydrogen flow rate were analytically made clear:

$$\frac{\dot{m}_{cl}}{\dot{m}_{\rm st}} \propto \eta_{cp}^{-0.2} q_\infty^{-0.2} \left(\frac{A_\infty}{A_1}\right)^{-0.2} \ell^{-0.2} \left[\frac{\gamma-1}{2} M_\infty^{2.2} + \left(1+\frac{\Delta T_r}{T_\infty} - \frac{T_w}{T_\infty}\right) M_\infty^{0.2}\right]$$

Acknowledgments

The authors acknowledge valuable advice from Hiroshi Miyajima and Kouichiro Tani of the National Aerospace Laboratory, Kakuda Research Center.

References

[1]Kanda, T., Masuya, G., and Wakamatsu, Y., "A Propellant Feed System of a Regeneratively Cooled Scramjet," *Journal of Propulsion and Power* (submitted for publication).

[2]Kanda, T., Masuya, G., and Wakamatsu, Y., "A System Analysis of a Regeneratively Cooled Scramjet," National Aerospace Lab., Tokyo, Japan, NAL TR-1002, 1989 (in Japanese).

[3]Buchmann, O. A., "Thermal-Structural Design Study of an Airframe-Integrated Scramjet," NASA CR-3141, 1979.

[4]Becker, J. V., "Prospects for Actively Cooled Hypersonic Transports," *Astronautics & Aeronautics,* Vol. 9, No. 8, 1971, pp. 32-39.

[5]Masuya, G., and Wakamatsu, Y., "Calculation of Scramjet Performance," National Aerospace Lab., Tokyo, Japan, NAL TR-987, 1988 (in Japanese).

[6]Trexler, C. A., "Inlet Performance of the Integrated Langley Scramjet Module," AIAA Paper 75-1212, 1975.

[7]Waltrup, P. J., Anderson, G. Y., and Stull, F. D., "Supersonic Combustion Ramjet (Scramjet) Engine Development in the United States," *Proceedings of the 3rd International Symposium of Air Breathing Engines,* DGLR-Fachbuch Nr. 6, 1976, pp. 836-862.

[8]Shapiro, A. H., *The Dynamics and Thermodynamics of Compressible Fluid Flow,* Ronald, New York, 1953, pp. 651-657.

[9]Northam, G. B., and Anderson, G. Y., "Supersonic Combustion Ramjet Research at Langley," AIAA Paper 86-0159, Jan. 1986.

[10]Mayer, E., "Analysis of Convective Heat Transfer in Rocket Nozzles," *ARS Journal,* Vol. 31, No. 7, 1961, pp. 911-917.

[11]Wakamatsu, Y., Kanda, T., Kanmuri, A., "Gas and Liquid Properties Calculation Code for LH_2/LO_2 Rocket Engine," National Aerospace Lab., Tokyo, Japan, NAL TM-564, 1987 (in Japanese).

[12]Anderson, G. Y., Eggers, J. M., Waltrup, P. J., and Orth, R. C., "Investigations of Step Fuel Injectors for an Integrated Modular Scramjet Engines," *Proceedings of 13th JANNAF Combustion Meeting,* Chemical Propulsion Information Agency, Applied Physics Lab., Laurel, MD, Sept. 1976.

[13]Sutton, G. P., and Ross, D. M., *Rocket Propulsion Elements,* 4th ed., Wiley, New York, 1976, pp. 282, 828.

[14]Wakamatsu, Y., Kanmuri, A., Toki, K., "Partial Bleed Expander Cycle for Low Thrust LOX/LH_2 Rocket Engine," National Aerospace Lab., Tokyo, Japan, NAL TR-837T, 1984.

[15]Niino, M., "Recent Development of the 'Functional Gradient Materials'," *Proceedings of the New Materials 88 Japan,* New Material Committee, Osaka, Japan, Oct. 1988, pp. 237-249.

[16]Schlicting, H., *Boundary Layer Theory,* 7th ed., McGraw-Hill, New York, 1979, pp. 597.

[17]Pinckney, S. Z., "Internal Performance Predictions for Langley Scramjet Engine Module," NASA TM X-74038, Jan. 1978.